Optical spectroscopy of $PrFe_3(BO_3)_4$: Crystal-field and anisotropic Pr-Fe exchange interactions

M. N. Popova and T. N. Stanislavchuk
Institute of Spectroscopy, Russian Academy of Sciences, Troitsk, 142190 Moscow Region, Russia

B. Z. Malkin
Kazan State University, 420008 Kazan, Russia

L. N. Bezmaternykh
L.V. Kirensky Institute of Physics, Siberian Branch, RAS, 660036 Krasnoyarsk, Russia

(Received 27 May 2009; revised manuscript received 11 September 2009; published 2 November 2009)

High-resolution polarized optical absorption spectra of $PrFe_3(BO_3)_4$ in the paramagnetic and antiferromagnetic phases are reported. The measured energies of the crystal-field (CF) levels within the $4f^2$ configuration of Pr^{3+} in the paramagnetic $PrFe_3(BO_3)_4$ are described by the CF model that involves the $4f^2/4f5d$ and $4f^2/4f6p$ configuration interactions. Ordering of Fe spins along the crystalline c axis below $T_N=32$ K is confirmed by the analysis of the spectra of Er^{3+} introduced as a probe into $PrFe_3(BO_3)_4$. To account for the observed changes in the optical spectra of Pr^{3+} at temperatures below T_N, in particular, for the shift of the CF levels, splitting of the CF doublets, and the appearance of forbidden lines, the Pr-Fe exchange Hamiltonian defined by seven parameters is considered. The theoretical approach has been tested by calculating the temperature dependence of the magnetic susceptibility. A good agreement between theory and optical and magnetic experimental data is found demonstrating the validity of the model used. The obtained results confirm that the model of the iron dimers inside the spiral chains of $Fe^{3+}(O^{2-})_6$ octahedrons introduced by us earlier for $NdFe_3(BO_3)_4$ and modified in the present work may serve as a basis for analyzing the low-temperature properties of other rare-earth iron borates.

DOI: 10.1103/PhysRevB.80.195101 PACS number(s): 78.30.Hv, 78.20.Bh, 71.70.Ch, 71.70.Gm

I. INTRODUCTION

The rare-earth (RE) iron borates $RFe_3(BO_3)_4$ (R=RE) have the trigonal noncentrosymmetric huntite-type structure that incorporates helical chains of edge sharing FeO_6 octahedrons interconnected by isolated RO_6 prisms and BO_3 triangles.[1] They belong to the same structural family as the famous aluminum borates $YAl_3(BO_3)_4$ (YAB) that, doped with Nd or Yb, are widely used in self-frequency doubling lasers (see, e.g., Refs. 2–4). A recent improvement of the crystal-growth technique for the RE iron borates[5] resulted in big perfect single crystals that demonstrated the same excellent physical characteristics and chemical stability as their aluminum relatives. This stimulated intensive investigation of $RFe_3(BO_3)_4$ single crystals by different methods. The growing interest of researchers is connected with rich and interesting magnetic properties of $RFe_3(BO_3)_4$ (Refs. 6–9) mediated by the existence of two interacting magnetic subsystems (Fe and RE). Moreover, it has recently been found that the RE iron borates are multiferroics.[10–13] This finding makes the mentioned compounds very interesting not only for research but also for possible applications.

Structural, magnetic, magnetoelastic, and magnetoelectric properties of $RFe_3(BO_3)_4$ are very different for different R^{3+} ions. While the crystal structure of the Pr and Nd iron borates is described by the $R32$ (D_3^7) space group down to at least 2 K,[12,14–16] the compounds with R^{3+} ions having smaller than Sm^{3+} ionic radii undergo a structural phase transition into also trigonal but less symmetric $P3_121$ (D_3^4) phase at temperatures T_S varying from 88 K [$EuFe_3(BO_3)_4$] to 420 K [$ErFe_3(BO_3)_4$].[15,17,18] Below the temperatures $T_N \sim 30-40$ K, $RFe_3(BO_3)_4$ with R=Nd,[14,19] Eu,[20] Gd,[21–23] Ho,[24,25] Er,[26] and diamagnetic Y (Refs. 25 and 26) order into the easy-plane antiferromagnetic structure while those with R=Pr,[12] Tb,[26,27] and Dy (Ref. 24) order into the easy-axis one. However, $GdFe_3(BO_3)_4$ and $HoFe_3(BO_3)_4$ undergo the spin-reorientation phase transitions into the easy-axis magnetic structure at the temperatures $T_R=9$ K (Refs. 13 and 21–23) and 5 K,[25] respectively. As for the magnetic-field-induced electric polarization, the greatest value has been observed for $NdFe_3(BO_3)_4$.[11]

For understanding the peculiarities of the magnetic and magnetoelectric properties of different RE iron borates, the knowledge of energies and wave functions of the crystal-field (CF) levels for RE ions and of the RE-Fe exchange interaction parameters is of fundamental importance. This knowledge can be achieved by doing the optical spectroscopy and performing the crystal-field calculations, and then on these grounds by evaluating the RE-Fe exchange parameters from an analysis of the optical spectrum changes in the magnetically ordered phase. In our recent work,[28] we estimated the Nd-Fe exchange integral in $NdFe_3(BO_3)_4$ from a comparison between the calculated and the measured ground-state splitting of the Nd^{3+} ion at temperatures T well below T_N. However, this approach, based on the assumption of the isotropic exchange, fails when considering the influence of the exchange interaction also on the excited states of a RE ion at $T<T_N$.

In a general case, the RE-Fe exchange interaction, including its anisotropic part, is defined by a set of coefficients in the expansion of the exchange Hamiltonian into series of irreducible tensor operators.[29] This set of coefficients comes from a comparison between the calculated and observed ex-

change splittings and shifts of energy levels in the spectrum of the RE^{3+} ion at low temperatures $T<T_N$.

In the present work, we focus on $PrFe_3(BO_3)_4$ which, on the one hand, has the same symmetric $R32$ structure as $NdFe_3(BO_3)_4$ but, on the other hand, comprises a non-Kramers Pr^{3+} ion (Nd^{3+} is a Kramers ion) with a singlet ground state.

We report on the high-resolution polarized absorption spectroscopy of Pr^{3+} in $PrFe_3(BO_3)_4$. The set of CF parameters was obtained from an analysis of the energy spectrum at temperatures $T>T_N$, with taking into account interactions between the ground $4f^2$ and excited $4f5d$ and $4f6p$ electronic configurations of the Pr^{3+} ion. Seven parameters of the two-particle Fe-Pr anisotropic exchange interaction were found from the fitting of the measured exchange splittings and shifts of the spectral lines. We use these parameters to model the experimental data[12] on the temperature dependence of the magnetic susceptibility of $PrFe_3(BO_3)_4$. Finally, we discuss some spectral peculiarities that originate from the electron-phonon coupling and the Pr-Fe exchange interaction. In particular, we present a detailed analysis of the recently observed[30] effect of the emergence of forbidden optical transitions at the temperature of the magnetic ordering in the $PrFe_3(BO_3)_4$ single crystal.

II. EXPERIMENT

Trigonal $PrFe_3(BO_3)_4$ single crystals, pure or Er (1%) doped, were grown in a bismuth trimolibdate $Bi_2Mo_3O_{12}$ based flux that has been used earlier for the growth of the $GdFe_3(BO_3)_4$ single crystals.[5] Direct probing of the flux melts

$$(100-n)\ \text{wt. \%}(Bi_2Mo_3O_{12}+pB_2O_3+qPr_2O_3)+n\ \text{wt. \%}PrFe_3(BO_3)_4$$

has shown that in the vicinity of the point $(p,q,n)=(3,0.6,25)$ the trigonal $PrFe_3(BO_3)_4$ is the high-temperature phase that crystallizes in a sufficiently broad range of temperatures but the saturation temperature does not exceed 970 °C. The seeds were obtained by spontaneous nucleation from the same flux. Large (10–15 mm) single crystals grown at the growth rate not more than 0.5 mm/day did not contain macroscopic inclusions of the flux melt, had glassy facets, were dark green in color, transparent, and had good optical quality. Oriented samples for spectral measurements have been prepared from such crystals. The samples were oriented using the crystal morphology and optical polarization methods. For optical measurements we used thin (0.1–0.15 mm) platelets cut either perpendicular or parallel to the c axis of the crystal.

High-resolution (up to 0.1 cm^{-1}) polarized temperature-dependent spectra were registered in the region 1500–23 000 cm^{-1} using a high-resolution Fourier spectrometer Bruker 125HR. To improve the signal-to-noise ratio in the spectral region 16 000–23 000 cm^{-1}, a green-blue optical filter was used. The sample was in a closed-cycle Cryomech ST403 cryostat at a fixed (±0.15 K) temperature between 3.5 and 300 K. Some measurements were performed using a helium vapor cryostat. We used either unpolarized light propagating along the c axis of the crystal ($\boldsymbol{k}\|c$, $\boldsymbol{E}$, $\boldsymbol{H}\perp c$—α polarization) or linearly polarized light incident perpendicular to the c axis ($\boldsymbol{k}\perp c$, $\boldsymbol{E}\|c$—π polarization and $\boldsymbol{E}\perp c$—σ polarization). $GdFe_3(BO_3)_4$ samples were also studied, to account for the broad absorption bands related to the Fe^{3+} ions (the Gd^{3+} ion has no optical transitions in the whole spectral range studied). These bands were then subtracted from the spectra of $PrFe_3(BO_3)_4$ to obtain the Pr^{3+}-related spectra.

To interpret the spectra of Pr^{3+} we used the selection rules for optical electric dipole (ED) and magnetic dipole (MD) transitions within a non-Kramers ion in the D_3 point symmetry group (positional symmetry of the Pr^{3+} ion in the trigonal $R32$ lattice). The allowed transitions are $\Gamma_1\leftrightarrow\Gamma_2$ (ED-π; MD-σ), $\Gamma_1\leftrightarrow\Gamma_3$ (ED-α, σ; MD-α, π), $\Gamma_2\leftrightarrow\Gamma_3$ (ED-α, σ; MD-α, π), and $\Gamma_3\leftrightarrow\Gamma_3$ (ED and MD for all polarizations). Here, Γ_k is the irreducible representation of the D_3 group. The first column of Table I contains information on how the crystal-field of the D_3 symmetry splits a particular Pr^{3+} free-ion level $^{2S+1}L_J$ into Γ_1 and Γ_2 singlets and Γ_3 doublets.

III. EXPERIMENTAL RESULTS AND DISCUSSION

A. Energies and symmetries of crystal-field levels

Figure 1 displays the absorption spectrum of Pr^{3+} in $PrFe_3(BO_3)_4$ in the whole spectral range studied. The spectrum consists of narrow spectral lines corresponding to the f-f transitions within the inner $4f^2$ electronic shell of Pr^{3+} shielded by the outer filled $5p$ and $5s$ shells. Figures 2–6 and 10 show the optical multiplets in more detail. Here and hereafter the spectral lines are designated according to the following notations: the CF levels of the ground multiplet are labeled by Roman numerals and those of a given excited multiplet—by capital letters (A, B, etc.).

As an example, the spectra in all the three polarizations (α, σ, and π) are shown in Fig. 2 for the optical multiplet $^3H_4\rightarrow{}^3F_2$. Perfect coincidence of the σ- and α-polarized spectra point to the purely electric dipole nature of this optical multiplet. Further, we note that the σ-polarized lines at 5031 and 5142.6 cm^{-1} diminish in intensity and then completely disappear with lowering the temperature. At temperatures $T>T_N$, these lines are displaced by 48 cm^{-1} to the low-frequency side from the lines marked IA and IC that remain at the lowest temperature when only the ground state is populated. Thus, the initial state for the spectral lines 5031 and 5142.6 cm^{-1} is the first excited CF level of the ground multiplet with the energy 48 cm^{-1} and they have to be labeled as IIA and IIC, respectively. We have checked that their intensity follows the population of the first excited CF level. The remaining three lines correspond to the optical transitions from the ground state to the $\Gamma_1+2\Gamma_3$ CF levels of the $^3F_2$ multiplet. If the ground state were the Γ_1 state, only two lines would be observed, because the $\Gamma_1\rightarrow\Gamma_1$ (and $\Gamma_2\rightarrow\Gamma_2$) transitions are *strictly forbidden.* Consulting the selection rules, we conclude that the symmetry of the ground state is Γ_2 and also assign the irreducible representations to the $^3F_2$ CF levels as shown in the second column of Table I. The absence of the IIB line in both σ- and π- polar-

TABLE I. The measured and calculated CF energies E and splittings Δ of the Γ_3 doublets. Calculated magnetic g factors and effective fields $B_{\text{eff}}=\Delta_{\text{exp}}/\mu_B g_{\parallel}$ are also given.

		Experiment		Theory			
Multiplet	Γ_i	E (cm^{-1}) $T=50$ K	Δ (cm^{-1}) $T=5$ K	E (cm^{-1}) $T>T_N$	$g_{\parallel}$	Δ (cm^{-1}) $T=5$ K	B_{eff} (kG)
1	2	3	4	5	6	7	8
$^3H_4$	2	0		0			
	1	48.5		48.1			
$2\Gamma_1+\Gamma_2+3\Gamma_3$	3	192		191.3	5.11	6.8	
	3	275		272.3	2.04	4.4	
	3	500		492.3	1.92	13.7	
	1	560		537.5			
$^3H_5$	3	2182.3	3.3	2181.0	7.68	3.3	9.2
	1	2275.2		2289.5			
$\Gamma_1+2\Gamma_2+4\Gamma_3$	2	2295.5		2300.4			
	3	2306.6		2300.5	8.94	2.4	
	3	?		2486.7	5.03	1.2	
	3	2588		2568.3	1.88	7.1	
	2	?		2623.6			
$^3H_6$	3	4292	12.1	4292.2	10.78	12	24.0
	3	4355.2	6	4384.0	8.48	6	15.1
$3\Gamma_1+2\Gamma_2+4\Gamma_3$	2	?		4483.4			
	1	4503.5		4506.3			
	2	?		4607.9			
	1	4641		4651.3			
	3	4748		4714.4	4.24	0.5	
	3	4819.3		4799.2	2.05	2.9	
	1	4850		4816.1			
$^3F_2$	3	5079		5082.5	1.03	3.8	
$\Gamma_1+2\Gamma_3$	1	5141.5		5119.7			
	3	5190.6	~4.6	5174.3	2.60	4.4	37.9
$^3F_3$	3	6471.1	1.8	6465.9	2.15	0.9	17.9
	2	6482.5		6482.4			
$\Gamma_1+2\Gamma_2+2\Gamma_3$	3	6508	2.5	6512.0	4.06	1.7	13.2
	2	6555		6542.2			
	1	6571.7		6566.8			
$^3F_4$	1	6863		6856.2			
	3	6885.8	~3.3	6887.9	3.47	4.8	20.3
$2\Gamma_1+\Gamma_2+3\Gamma_3$	2	6957.3		6941.8			
	3	6957.5	13.5	6965.0	3.21	13.3	90
	1	7099.5		7095.2			
	3	7107.8		7104.3	7.16	11	
$^1G_4$	1	9728.5		9722.9			
	3	9776.7		9773.4	2.59	5.1	
$2\Gamma_1+\Gamma_2+3\Gamma_3$	3	9925.6	8.1	9953.4	3.59	8.4	48.3
	2	9946		9923.5			
	3	10113.8		10157	5.45	4.0	
	1	10193.4		10223			
$^1D_2$	1	16491		16547			

TABLE I. (*Continued.*)

		Experiment		Theory			
Multiplet	Γ_i	E (cm^{-1}) T=50 K	Δ (cm^{-1}) T=5 K	E (cm^{-1}) $T>T_N$	$g_\parallel$	Δ (cm^{-1}) T=5 K	B_{eff} (kG)
1	2	3	4	5	6	7	8
$\Gamma_1+2\Gamma_3$	3	16791	~3.3	16800	1.26	1	56.0
	3	17080		17048	0.80	1	
$^3P_0\Gamma_1$	1	20567		20545			
$^3P_1+^1I_6$	2	20848		20851			
	1	20856		20859			
$3\Gamma_1+3\Gamma_2+5\Gamma_3$	3 $^3P_1$	21100	9.2	21097	3.21	9	64.7
	2 $^3P_1$	21280		21272			
	3	21382		21368	7.96	2	
	1	21420		21431			
	3	21453		21446	3.25	1	
	2	?		21697			
	3	?		21707	5.15	1	
	1	21760		21746			
	3	21810		21767	5.83	6	
$^3P_2$	1	22193		22196			
	3	22334		22310	2.42	8	
$\Gamma_1+2\Gamma_3$	3	?		22434	5.53	13	
$^1S_0$	1	?		45128			
4*f*5*d*				44377–67610			
4*f*6*p*				117080–132000			

ized 50 K spectrum points to the Γ_1 symmetry of the level at 48 cm^{-1}.

It should be noted that for the paramagnetic $PrFe_3(BO_3)_4$, the number of spectral lines originating from the ground state always equals to the number of irreducible representations in the first column of Table I after deduction of the number of Γ_2 irreducible representations. This fact convincingly confirms the Γ_2 symmetry of the ground state. The π-polarized lines correspond to the $\Gamma_2 \leftrightarrow \Gamma_1$ optical transitions but the σ-polarized ones originate from the Γ_2 (or Γ_1) $\rightarrow \Gamma_3$ transitions. The magnetic dipole contribution was observed only for the $^3H_4 \rightarrow {}^3H_5$ transition that is allowed in the free Pr^{3+} ion as magnetic dipole one and for the spin-forbidden $^3H_4 \rightarrow {}^1G_4$ transitions. In these cases, the $\Gamma_2 \rightarrow \Gamma_1$ transition,

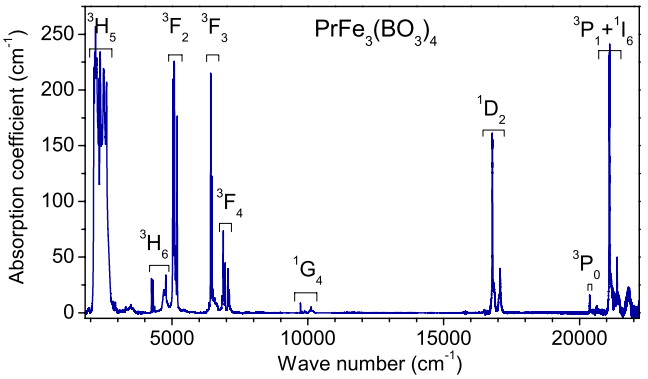

FIG. 1. (Color online) Absorption spectrum of Pr^{3+} in $PrFe_3(BO_3)_4$ at the temperature 50 K.

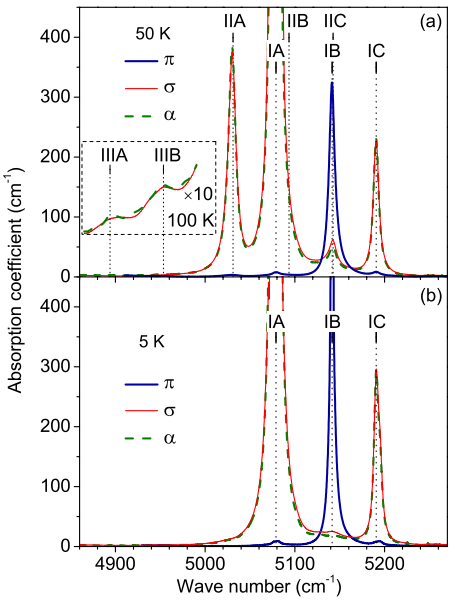

FIG. 2. (Color online) Polarized absorption spectra of the $^3F_2$ multiplet in $PrFe_3(BO_3)_4$ at the temperatures of (a) 100 and 50 K and (b) 5 K in α, π, and σ polarizations.

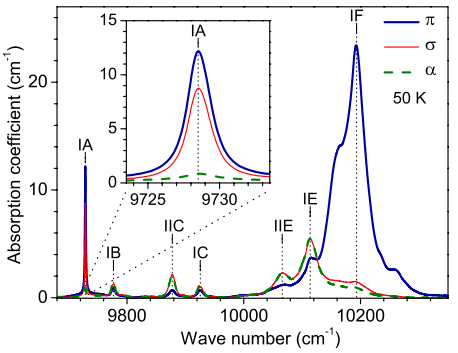

FIG. 3. (Color online) Polarized 50 K absorption spectra of the $^1G_4$ multiplet. Inset shows in more detail the IA $\Gamma_2 \rightarrow \Gamma_1$ optical transition demonstrating both electric dipole and magnetic dipole contributions.

in particular, was observed also in the σ polarization but its assignment was confirmed by the absence of the corresponding line in the α polarization. Inset of Fig. 3 gives an example of such a line. Figure 4 shows the $^3H_4 \rightarrow {}^3P_0$ optical multiplet which consists, at low temperatures, of a single π-polarized $\Gamma_2 \rightarrow \Gamma_1$ line. With rising the temperature, the σ-polarized line shifted by 192 cm^{-1} appears. It originates from the second excited Γ_3 CF sublevel of the ground state. The low-frequency −48 cm^{-1} satellite of the $\Gamma_1(^3P_0)$ line, $\Gamma_1 \rightarrow \Gamma_1$, is absent, in complete agreement with selection rules. The energies and symmetries of the CF levels, as determined from the temperature-dependent polarized absorption spectra of $PrFe_3(BO_3)_4$, are listed in Table I.

Interaction of the $4f$ electrons of the RE ion with lattice vibrations results in broadening and shifts of spectral lines and in the appearance of vibronic transitions. Below, we point to several peculiarities in the spectra of $PrFe_3(BO_3)_4$ originating from this interaction.

First, as the lowest levels in those $^{2S+1}L_J$ multiplets that are separated by a large energy gap from the lower lying levels do not suffer from phonon relaxation at low temperature, the corresponding spectral lines are the narrowest ones. For example, in the $^1G_4$ spectral multiplet shown in Fig. 3, the full width at half height of the line IA is only 0.5 cm^{-1} at 5 K while it equals 30 cm^{-1} for the line IE.

Second, relatively weak structured wings accompany some of the strong spectral lines. An example of such wing

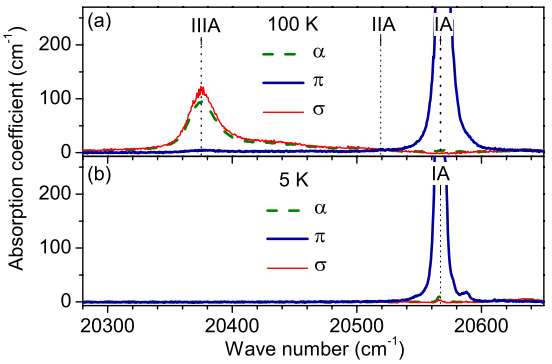

FIG. 4. (Color online) Polarized $^3H_4 \rightarrow {}^3P_0$ absorption of $PrFe_3(BO_3)_4$ at different temperatures.

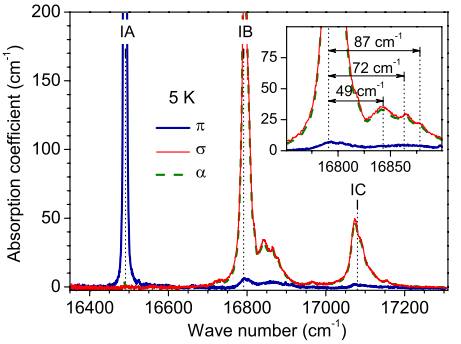

FIG. 5. (Color online) Polarized 5 K absorption spectrum of the $^1D_2$ multiplet. Inset: vibronic satellites of the line IB corresponding to the transition $^3H_4(\Gamma_1) \rightarrow {}^1D_2(\Gamma_3)$.

can be seen in the $^1D_2$ multiplet (Fig. 5). The distances between the main line and the peaks in the wing (see inset in Fig. 5) are close to the measured frequencies of the Raman and infrared modes.[15,16,31]

Third, several lines exhibit a doublet structure (see, e.g., the lines IF in Fig. 3 and IC in Fig. 5) or even more complex structure (ID and IE in Fig. 6). This could be caused by the resonance of a given electronic CF state and a mixed electron-phonon state associated to another electronic CF state with lower energy.[32] In all the cases of the observed line structure the terminal level of the optical transition is situated by 300–400 cm^{-1} above some other CF level. Probably, this spectral interval corresponds to a narrow maximum in the density of phonon states in $PrFe_3(BO_3)_4$.

B. Magnetic ordering

With lowering the temperature, the $\Gamma_2 \rightarrow \Gamma_3$ and $\Gamma_1 \rightarrow \Gamma_3$ spectral lines split into two components. Figure 7 gives an

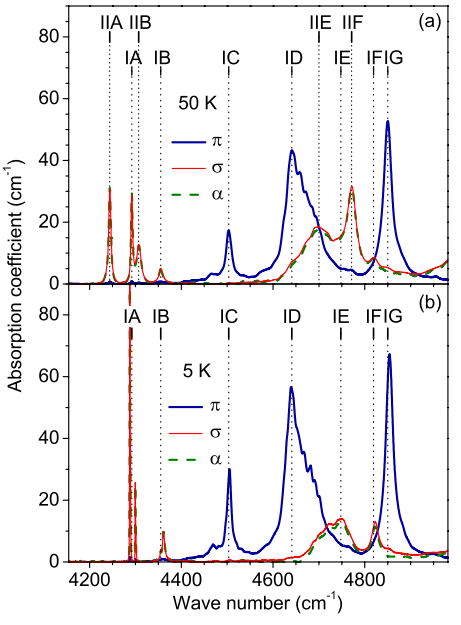

FIG. 6. (Color online) Polarized 50 K absorption spectrum of the $^3H_6$ multiplet at the temperatures of (a) 50 K and (b) 5 K in α, π, and σ polarizations.

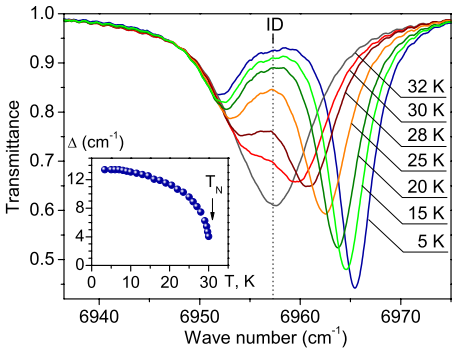

FIG. 7. (Color online) The spectral line ID $\Gamma_2^I(^3H_4) \rightarrow \Gamma_3^D(^3F_4)$ in the spectrum of $PrFe_3(BO_3)_4$ at different temperatures. Inset shows the temperature dependence of the line splitting Δ.

example of a split line. The temperature dependence of the splitting points to a second-order phase transition (see inset of Fig. 7). Both the structural and the magnetic phase transitions may cause a splitting of a non-Kramers Γ_3 doublet. To check the nature of the observed phase transition, we studied the spectra of the Er^{3+} probe ion in $PrFe_3(BO_3)_4$. The only perturbation that splits the CF energy levels of this ion (Kramers doublets) is the magnetic field (external or the exchange one that acts upon the RE ion in the magnetically ordered phase). The temperature-dependent splitting of Er^{3+} spectral lines [represented in Figs. 8(a) and 8(b)] unambiguously shows that we deal with the magnetic phase transition. The observed spectral pattern of the split line corresponds to the splitting of the Kramers doublets and cannot be explained in another way. In particular, the intensity of the spectral components 1′a and 1′a′ diminishes at the lowest temperatures [see Fig. 8(a) and the scheme in Fig. 8(c)]. The splittings $\Delta = 1.5$ cm^{-1} and $\Delta_A = 3.8$ cm^{-1} at $T = 5$ K, for the ground and the excited Kramers doublets, respectively, follow from the spectra of Fig. 8(a).

We note that the spectra of the Er^{3+} probe not only elucidate the magnetic nature of the observed phase transition but also give a possibility to determine the type of the magnetic structure within the magnetically ordered iron subsystem. We can compare the spectra of the Er^{3+} probe in $PrFe_3(BO_3)_4$ and in $GdFe_3(BO_3)_4$ which is known to undergo the spin-reorientation first-order phase transition at $T_R = 9$ K, from the easy-plane magnetic structure above T_R to the easy-axis one below T_R.[21] In $GdFe_3(BO_3)_4$ the spectrum of the Er^{3+} probe changes drastically at T_R [see, e.g., Fig. 8(d) and Refs. 24 and 26]. The spectrum of the Er^{3+} ion in $PrFe_3(BO_3)_4$ is similar to the spectrum of Er^{3+} in $GdFe_3(BO_3)_4$ below T_R [see Fig. 8(a)], thus pointing to the easy-axis magnetic structure of the ordered Fe^{3+} magnetic moments. This conclusion is in agreement with recent results of the magnetic measurements.[12]

Figure 9 compares the temperature dependence of the splitting of the Pr^{3+} Γ_3 doublet at 6957 cm^{-1}, $\Delta(T)$, and the temperature variation in the magnetic moment of the Fe^{3+} ions in the easy-axis magnet $TbFe_3(BO_3)_4$ at $T < T_N$, $\boldsymbol{M}_{Fe}$, obtained from the neutron scattering data.[27] One can clearly see that the splitting $\Delta(T)$ is proportional to $\boldsymbol{M}_{Fe}$.

To explain this dependence, we note that in the compounds containing both *d* ions (Fe^{3+} in our case) and *f* ions

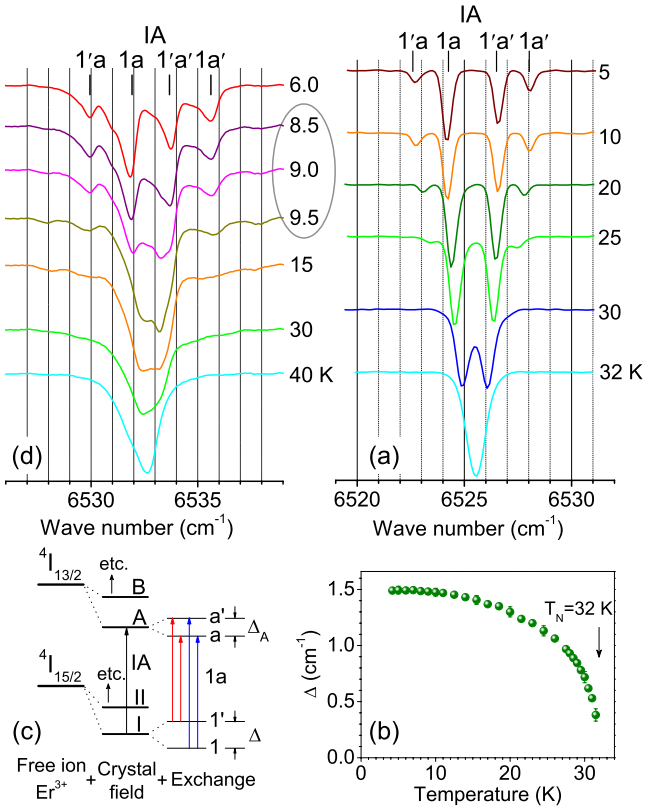

FIG. 8. (Color online) The line IA in the spectra of the $^4I_{15/2} \rightarrow {}^4I_{13/2}$ transition of Er^{3+} probe in (a) $PrFe_3(BO_3)_4$ and (d) $GdFe_3(BO_3)_4$, (b) the temperature dependence of the ground-state splitting for Er^{3+} in $PrFe_3(BO_3)_4$, and (c) the scheme of splitting of Er^{3+} Kramers doublets due to the Er-Fe exchange interaction.

(Pr^{3+} and Er^{3+}), the strongest interactions are those within the *d*-magnetic subsystem, then follow *f*-*d* interactions and still less weak *f*-*f* ones.[33] In iron borates, RO_6 prisms do not have common oxygen ions; because of that, magnetic interactions between the RE ions have mainly the dipole nature and are especially weak. Thus, in the case of the isotropic *f*-*d* exchange interaction, a RE^{3+} ion (Pr^{3+} or Er^{3+}) in the magnetically ordered state of $PrFe_3(BO_3)_4$ experiences the perturbation $V = \mu_B g_0 \boldsymbol{J}\boldsymbol{B}_{ex}$ where μ_B is Bohr magneton, g_0 is Lande factor, $\boldsymbol{J}$ is the angular momentum operator, $\boldsymbol{B}_{ex} = \lambda \boldsymbol{M}_{Fe}$ is the effective exchange magnetic field, and λ is the molecular-field constant. In the crystallographic system of coordinates, only one component of the *g* tensor of the non-Kramers doublet, $g_{zz} = g_\parallel$, corresponding to the crystal symmetry axis ($z \parallel c$), is nonzero, and the Zeeman splitting of the Γ_3 doublet reads

$$\Delta(T) = \mu_B g_\parallel B_{ex,z} = \mu_B g_\parallel \lambda M_{Fe,z}(T). \quad (1)$$

Thus, the splitting $\Delta(T)$ is proportional to the magnetic moment $M_{Fe,z}$ of the Fe^{3+} ion along the crystallographic *c* axis which is *the order parameter of the magnetic phase transition*. Table I (column 4) lists the splittings of the Pr^{3+} different Γ_3 doublets observed at the temperature 5 K.

As for a possible contribution of the magnetostriction to the splitting, we note that the symmetry analysis for the crystal class 32 (i) points to the absence of the spontaneous low-

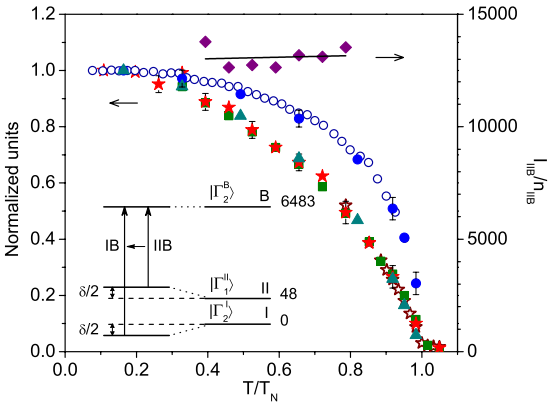

FIG. 9. (Color online) The splitting Δ of the $\Gamma_3^D(^3F_4)$ level (balls), $\Delta(5\ \mathrm{K})=13.5\ \mathrm{cm}^{-1}$; the same splitting squared (triangles), the increase δ of the energy gap between the lowest two levels Γ_2^{I} and Γ_1^{II} of the ground multiplet (squares), $\delta(5\ \mathrm{K})=4.6\ \mathrm{cm}^{-1}$; ratios I/n of the integrated line intensity I to the relative population n of the initial level of the optical transition for the transitions $\Gamma_2^{\mathrm{I}}\rightarrow\Gamma_2^B(^3F_3)$ (open stars), $\Gamma_2^{\mathrm{I}}\rightarrow\Gamma_2^B(^3P_1+{}^1I_6)$ (stars), $\Gamma_1^{\mathrm{II}}\rightarrow\Gamma_2^B(^3F_3)$ (diamonds); and the spontaneous iron magnetic moment in $TbFe_3(BO_3)_4$, M_{Fe} measured by the neutron scattering (Ref. 27) (open circles), $M_{\mathrm{Fe}}(5\ \mathrm{K})=4.4\ \mu_B$, as functions of the normalized temperature T/T_N. Inset shows the scheme of relevant energy levels of the Pr^{3+} ion.

symmetry striction in the case of the magnetic moments $\boldsymbol{M}_{\mathrm{Fe}}$ ordered along the c axis and, moreover, (ii) shows that at any orientation of the magnetic moments the dependence of the striction on M_{Fe} does not contain linear in M_{Fe} terms.[10] This confirms a purely exchange nature of the observed splitting $\Delta(T)$.

It should be also noted that centers of gravity of the split doublets and some spectral lines corresponding to singlet-singlet $\Gamma_1\leftrightarrow\Gamma_2$ transitions exhibit relatively strong shifts (up to 4.5 cm^{-1}) in the temperature range from T_N down to 5 K. Figure 9 shows the temperature dependence of the increase $\delta(T)=E_{\mathrm{II,I}}(T<T_N)-E_{\mathrm{II,I}}(T_N)$ of the energy gap $E_{\mathrm{II,I}}=E(\Gamma_1^{\mathrm{II}})-E(\Gamma_2^{\mathrm{I}})$ between the ground-state Γ_2^{I} and the first excited state Γ_1^{II} (schematically represented in inset of Fig. 9) and compares it with the $\Delta(T)$ and $\Delta^2(T)$ dependences. The increase in the gap is proportional to $\Delta^2(T)$ and, thus, to the square of the magnetic order parameter [see Eq. (1)]. Such behavior can be easily understood in the framework of the perturbation theory.

Indeed, the first-order corrections to the energies of the Γ_1 and Γ_2 singlets due to the perturbation V vanish but the second-order corrections,

$$\Delta E(\Gamma_1^{\mathrm{II}}) = -\Delta E(\Gamma_2^{\mathrm{I}}) = \tfrac{1}{2}\delta(T) = |\alpha(T)|^2 E_{\mathrm{II,I}}(T_N), \qquad (2)$$

with

$$\alpha(T) = \frac{\mu_B g_0 \langle\Gamma_1^{\mathrm{II}}|J_Z|\Gamma_2^{\mathrm{I}}\rangle}{E_{\mathrm{II,I}}(T_N)} \lambda M_{\mathrm{Fe},z}(T), \quad |\alpha| < 1, \qquad (3)$$

are proportional to the square of the magnetic order parameter. In Eq. (2), a contribution from the Γ_1 state at 560 cm^{-1} (see Table I) is neglected; all the other CF states of the $^3H_4$ ground multiplet (which are the Γ_3 states) do not contribute.

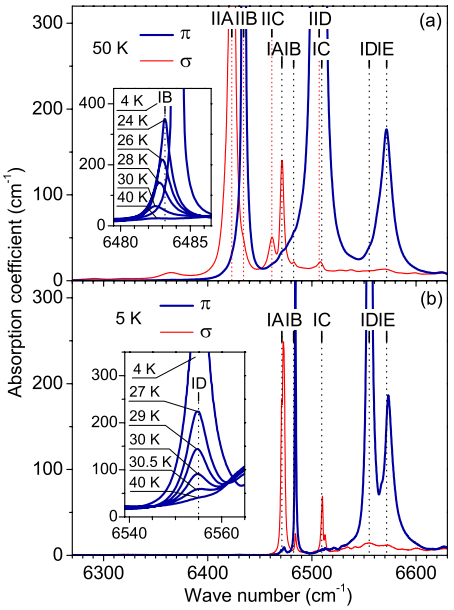

FIG. 10. (Color online) Emergent lines in the low-temperature spectrum of the $^3F_3$ multiplet. The Insets show in detail the rise of the lines (a) IB and (b) ID below T_N.

Together with the second-order corrections to the energies, one finds the first-order corrections to the wave functions, $|\Gamma_2^{\mathrm{I}}(T)\rangle=(1+|\alpha(T)|^2)^{-1/2}(|\Gamma_2^{\mathrm{I}}\rangle+\alpha(T)|\Gamma_1^{\mathrm{II}}\rangle)$. The entanglement of the Γ_1 and Γ_2 states at $T<T_N$ breaks the selection rules for optical transitions. Strictly forbidden $\Gamma_2\rightarrow\Gamma_2$ spectral lines should appear below T_N, borrowing their intensity from the allowed $\Gamma_1\rightarrow\Gamma_2$ transitions. An example of such emergent lines is shown in Fig. 10 that displays the optical multiplet $^3H_4\rightarrow{}^3F_3$. At elevated temperatures $T>T_N$, transitions from the lowest two levels Γ_2^{I} and Γ_1^{II} of the ground multiplet to the Γ_3 and Γ_1 sublevels of the $^3F_3$ multiplet are observed, together with two strong π-polarized lines IIB and IID of the $\Gamma_1^{\mathrm{II}}\rightarrow\Gamma_2$ transitions. The $\Gamma_2\rightarrow\Gamma_2$ lines are absent, in a complete agreement with the selection rules. However, below T_N, two additional π-polarized lines, IB and ID, emerge and rise in intensity with further lowering the temperature. The lines IB and ID arise at the positions shifted precisely 48 cm^{-1} to higher frequencies from the lines IIB and IID, respectively, and, thus, have to be assigned to the *forbidden* $\Gamma_2\rightarrow\Gamma_2$ transitions. Insets of Fig. 10 represent the lines IB and ID at different temperatures $T<T_N$. Both lines are saturated in a 0.15-mm-thick sample at low temperatures, but we failed to prepare a thinner sample. To measure the intensity of an emergent line in the whole temperature interval $T<T_N$, we have chosen the weak line at 21 280 cm^{-1} corresponding to the $\Gamma_2^{\mathrm{I}}\rightarrow\Gamma_2^D(^3P_1+{}^1I_6)$ optical transition. Stars in Fig. 9 represent the integral intensity I of this line divided by the relative population of the ground level $n_{\mathrm{I}}(T)$. Open stars refer to the same quantity for the line IB of Fig. 10, in the temperature interval where correct measurements of the intensity were possible. One can see that the quantity I/n_{I} for emergent lines follows the same temperature dependence as the increase $\delta(T)$ of the energy gap between the lowest states Γ_2^{I} and Γ_1^{II} and is thus also proportional to the square of the magnetic order parameter.

Neglecting a possible modification of the wave function $|\Gamma_2^B\rangle$ at $T<T_N$ [which is justified by a large distance between the level B ($^3F_3$) and the nearest Γ_1 level E ($^3F_3$)—see Table I], we obtain the following relation between the intensities of the forbidden (IB) and allowed (IIB) transitions

$$\frac{I_{\mathrm{IB}}(T)}{n_{\mathrm{I}}(T)} = |\alpha(T)|^2 \frac{I_{\mathrm{IIB}}(T)}{n_{\mathrm{II}}(T)}. \tag{4}$$

Here, $n_{\mathrm{II}}(T)$ is the relative population of the level Γ_1^{II} which is determined by Boltzmann distribution. From Eq. (2), using the measured shift $\delta(T=26\ \mathrm{K})=1.8\pm0.2\ \mathrm{cm}^{-1}$ of the IB line relative to the IIB line, with respect to the energy gap between the ground state Γ_2^{I} and the first excited state Γ_1^{II} at $T=33\ \mathrm{K}>T_N$, $E_{\mathrm{II,I}}=48.9\pm0.1\ \mathrm{cm}^{-1}$, we obtain $|\alpha|^2=0.018\pm0.002$. The value $|\alpha|^2=0.027\pm0.006$ is obtained after substitution of the intensities $I_{\mathrm{IB}}/n_{\mathrm{I}}=360\pm40\ \mathrm{cm}^{-2}$, $I_{\mathrm{IIB}}/n_{\mathrm{II}}=13\,000\pm1000\ \mathrm{cm}^{-2}$ measured at the same temperature into Eq. (4). The discrepancy between these two values is almost within the precision of measurements. However, an additional contribution to the relative line shift due to spontaneous magnetostriction and a non-negligible effect of the exchange interaction on the wave function of the final state Γ_2^B ($^3F_3$) of the considered optical transition are also possible.

Using the expression for α from Eq. (2) and the value $g_0\langle\Gamma_1^{\mathrm{II}}|J_z|\Gamma_2^{\mathrm{I}}\rangle=2.234$ obtained from the crystal-field calculations (see Sec. IV A), we get the estimates for the maximum value of the exchange field $B_{\mathrm{ex}}(5\ \mathrm{K})=98\pm4$ kG or $B_{\mathrm{ex}}(5\ \mathrm{K})=120\pm13$ kG from the measurements of $\delta(T)$ or of the intensity of the emergent line IB, respectively. These values are close to the value $B_{\mathrm{ex}}\approx115$ kG obtained from the magnetic susceptibility measurements in Ref. 12.

Thus, the suggested mechanism explains well the discovered effect of the appearance of forbidden spectral transitions at the magnetic ordering of a crystal. The effective exchange magnetic field mixes the states of different symmetries. As a result, a formerly forbidden optical transition borrows the intensity from a close in energy allowed transition (see the scheme in the inset of Fig. 9).

IV. EFFECTIVE HAMILTONIAN OF THE Pr^{3+} IONS

A. Crystal-field and configuration interactions

The measured energy spectrum of the Pr^{3+} ions in $PrFe_3(BO_3)_4$ in the paramagnetic phase was analyzed using the Hamiltonian $H_{\mathrm{Pr}}^{(p)}=H_{\mathrm{FI}}+H_{\mathrm{CF}}$, where H_{FI} is the free-ion Hamiltonian and H_{CF} corresponds to the interaction with the crystal-field. At the Pr^{3+} sites with the D_3 symmetry, in the Cartesian system of coordinates with the z axis along the crystallographic c axis and the x axis along the crystallographic a axis (which is the C_2 symmetry axis), the even component of the CF Hamiltonian that determines the CF splitting of the $4f^2$ states is defined by six independent real CF parameters B_q^p: $(p=2,4,6; p\geq|q|, q=0,-3,6)$,

$$H_{\mathrm{CF}}^{(e)} = \sum_k \{B_0^2 C_0^{(2)}(k) + B_0^4 C_0^{(4)}(k) + B_0^6 C_0^{(6)}(k) + iB_{-3}^4[C_{-3}^{(4)}(k) + C_3^{(4)}(k)] + iB_{-3}^6[C_{-3}^{(6)}(k) + C_3^{(6)}(k)] + B_6^6[C_{-6}^{(6)}(k) + C_6^{(6)}(k)]\}. \tag{5}$$

Here the sum is taken over $4f$ electrons, $C_q^{(p)}(k)$ is the spherical tensor operator of rank p. Values of the free-ion parameters were taken from literature for impurity Pr^{3+} ions in the oxygen surrounding in YPO_4.[34] Values of the CF parameters were obtained by fitting the eigenvalues of the Hamiltonian $H_{\mathrm{Pr}}^{(p)}$ to the measured CF energies. The initial set of the B_q^p parameters was taken from our previous study on $NdFe_3(BO_3)_4$.[28] By varying these parameters up to 20%, we could not remove pronounced discrepancies between the calculated and measured CF energies for the multiplets with zero value of the total spin ($^1G_4$, $^1D_2$). This problem in the analysis of the Pr^{3+} spectra in other dielectric crystals was earlier discussed in the literature.[34,35] In particular, it has been shown that mixing of the ground configuration $4f^2$ with the excited configurations $4f5d$ and, especially, $4f6p$ can induce relative shifts of CF energy levels comparable to the largest differences (up to 100 cm^{-1}) between the experimental energies and the results of the numerical diagonalization of the Hamiltonian $H_{\mathrm{Pr}}^{(p)}$ in the space of states of the $4f^2$ configuration only.

So, our next step was to take into account the $4f^2/4f5d$ and $4f^2/4f6p$ configuration interactions explicitly. We would like to note at once that in the case of Pr^{3+} in $PrFe_3(BO_3)_4$ too, a much better description of the measured CF energies for the $^1G_4$ multiplet was achieved when performing the calculations in the total space of $91(4f^2)+140(4f5d)+84(4f6p)=315$ states. The ground $4f^2$ configuration is coupled to the $4f6p$ configuration by the electrostatic interaction and by the even crystal field and to the $4f5d$ configuration by the odd crystal field

$$H_{\mathrm{CF}}^{(odd)} = \sum_k \{B_3^3[C_{-3}^{(3)}(k) - C_3^{(3)}(k)] + B_3^5[C_{-3}^{(5)}(k) - C_3^{(5)}(k)]\}. \tag{6}$$

To account for the $4f^2$-$4f6p$ electrostatic interaction, we used the Slater parameters $F^2(f,f,f,p)=-4886$ and $F^4(f,f,f,p)=-2968\ \mathrm{cm}^{-1}$.[34,35] Reasonable values of the additional even CF parameters $B_0^2(f,p)=1600$, $B_0^4(f,p)=-5500$, and $B_{-3}^4(f,p)=6000\ \mathrm{cm}^{-1}$ were obtained from fitting of the $^1G_4$ multiplet CF splitting. Parameters of the odd crystal field $B_3^3(f,d)=2110$ and $B_3^5(f,d)=2170\ \mathrm{cm}^{-1}$ were calculated in the framework of the point charge model. The final set of CF parameters for the ground configuration is as follows (the initial values of CF parameters corresponding to the Nd^{3+} ions in $NdFe_3(BO_3)_4$ (Ref. 28) are in brackets): $B_0^2=556$ (551), $B_0^4=-1447$ (−1239), $B_{-3}^4=867$ (697), $B_0^6=534$ (519), $B_{-3}^6=165$ (105), and $B_6^6=376$ (339) cm^{-1}. The calculated CF energies are compared with the experimental data in Table I.

Using the wave functions found as eigenvectors of the Hamiltonian $H_{\mathrm{Pr}}^{(p)}$, we have calculated the magnetic spectro-

scopic factors $g_{\|}$ for the Γ_3 levels (see Table I, column 6). Substituting the measured values of the splitting Δ of the Γ_3 doublets and the calculated g factors into Eq. (2), we estimated the corresponding effective exchange magnetic field and found that B_{eff} differs substantially for different Γ_3 states (see column 8 of Table I). The reason is that because of an essential anisotropy of the RE-Fe exchange interaction, the level splittings cannot be accounted for by a single parameter (effective exchange magnetic field).[29] The correct Hamiltonian for the Pr-Fe exchange interaction is presented in the next section.

B. Hamiltonian of the Pr-Fe exchange interaction

According to results of the neutron diffraction studies of the magnetic structures in RE iron borates, the coupling between the nearest Fe^{3+} ions is antiferromagnetic within the spiral Fe-O-Fe chains along the c axis and ferromagnetic in the planes normal to this axis.[14,25,27] In the magnetically ordered phase, the unit cell doubles along the c axis, and directions of the magnetic moments of the Fe^{3+} ions are governed by the magnetic anisotropy of the RE ions. In $PrFe_3(BO_3)_4$ magnetic moments of the Pr^{3+} and Fe^{3+} ions are collinear with the c axis.[12]

The exchange interaction between the RE ion and the S-state (Fe^{3+}) ion has the form[29]

$$H_{\text{RE-Fe}} = \sum_k A(\boldsymbol{l}_k)\boldsymbol{s}_k \cdot \boldsymbol{S}_{\text{Fe}}, \tag{7}$$

where $\boldsymbol{l}_k$ and $\boldsymbol{s}_k$ are the orbital and spin moments, respectively, of the kth $4f$ electron, and $\boldsymbol{S}_{\text{Fe}}$ is the spin moment of the Fe^{3+} ion. The exchange potential operator $A(\boldsymbol{l}_k)$ that describes the dependence of the exchange energy on the orbital state of the RE ion can be expanded in a series of spherical tensor operators. In the framework of the mean-field approximation, neglecting fluctuations of the iron spin moments, we substitute the average value of the spin moment $\langle \boldsymbol{S}_{\text{Fe}} \rangle$ for the dynamic variable $\boldsymbol{S}_{\text{Fe}}$. Summing expression (7) over the six Fe^{3+} nearest neighbors to a Pr^{3+} ion, which are magnetically equivalent, we obtain the exchange potential of trigonal symmetry with the structure of the CF Hamiltonian (5). The exchange Hamiltonian for the Pr^{3+} ion may be written as $H_{\text{exch}} = -\boldsymbol{F} \cdot \boldsymbol{M}_{\text{Fe}}$, where $\boldsymbol{M}_{\text{Fe}} = -g\mu_B \langle \boldsymbol{S}_{\text{Fe}} \rangle (g=2)$ and

$$\begin{aligned}\boldsymbol{F} = \frac{1}{2\ \mu_B} \sum_k \{ & a_0^{(0)} + a_0^{(2)} C_0^{(2)}(k) + a_0^{(4)} C_0^{(4)}(k) + a_0^{(6)} C_0^{(6)}(k) \\ & + i a_{-3}^{(4)} [C_3^{(4)}(k) + C_{-3}^{(4)}(k)] + i a_{-3}^{(6)} [C_3^{(6)}(k) + C_{-3}^{(6)}(k)] \\ & + a_6^{(6)} [C_6^{(6)}(k) + C_{-6}^{(6)}(k)] \} \boldsymbol{s}_k. \end{aligned} \tag{8}$$

In absence of the external magnetic field and at temperatures $T < T_N$, the subsystem of the Pr^{3+} ions contains two sublattices with antiparallel magnetic moments induced by the Pr^{3+}-Fe^{3+} exchange interaction. The Hamiltonian for the Pr^{3+} ions is then written as follows:

$$H_{\text{Pr}}^{(\mp)} = H_{\text{FI}} + H_{\text{CF}} \mp F_z M_{\text{Fe},z}, \tag{9}$$

where $M_{\text{Fe},z} = -g\mu_B \langle S_{\text{Fe},z} \rangle$ is the order parameter of the magnetic phase transition. The energy spectrum of the Pr^{3+} ions at the temperature 5 K was obtained using numerical diagonalization of the matrix of the Hamiltonian (9) calculated in the basis of the two-electron Slater determinants for the $4f^2$, $4f5d$ and $4f6p$ configurations. For $M_{\text{Fe},z}$, we adopted the value 4.8 μ_B at 5 K,[14] slightly smaller than the saturation moment 5 μ_B. The values of the seven parameters of the exchange potential $a_0^{(0)} = 0.708$, $a_0^{(2)} = 24.10$, $a_0^{(4)} = -28.55$, $a_0^{(6)} = 29.13$, $a_{-3}^{(4)} = 0.77$, $a_{-3}^{(6)} = -26.82$, and $a_6^{(6)} = -38.97$ cm^{-1} were found from a comparison of the calculated splittings of the Γ_3 doublets and the temperature-dependent gap between the lowest Γ_1 and Γ_2 sublevels of the ground multiplet $^3H_4$ with the experimental data (see Table I, columns 4 and 7).

If we compare contributions of different terms in the effective exchange potential (12) to the exchange splittings of the Pr^{3+} doublet levels in $PrFe_3(BO_3)_4$ the result is that the *contributions of the anisotropic terms* to the splittings are, as a rule, *comparable to or even larger than those of the isotropic term* defined by the $a_0^{(0)}$ parameter. In this context, one should keep in mind that the estimate of the effective exchange field obtained in the Sec. III B and in Ref. 12 refers only to the pair of the lowest two levels of the Pr^{3+} ion in $PrFe_3(BO_3)_4$.

Next, we consider the influence of the exchange interaction upon the intensities of the optical transitions. Integral intensities of the electric dipole transitions between CF states of the ground $4f^2$ configuration are proportional to squared moduli of the corresponding matrix elements of the electric dipole moment of the Pr^{3+} ion. For the π-polarized radiation, only the z component of the dipole moment

$$\begin{aligned} D_z = \sum_k \{ & e r_k C_0^{(1)}(k) + b_3^4 [C_{-3}^{(4)}(k) - C_3^{(4)}(k)] \\ & + b_3^6 [C_{-3}^{(6)}(k) - C_3^{(6)}(k)] + i b_{-6}^6 [C_{-6}^{(6)}(k) - C_6^{(6)}(k)] \} \end{aligned} \tag{10}$$

is relevant (where e is the electron charge and r_k is the radius of an electron). The first (odd) term in Eq. (10) has nonzero matrix elements within the space of states of the ground configuration due to its mixing with the $4f5d$ configuration in the odd crystal field, the additional (even) terms correspond to the interaction of the Pr^{3+} ion with the crystal lattice polarized by the incident radiation.[36] For simplicity, we have restricted our consideration to the polarization of oxygen sublattices only. The reasonable value of the O^{2-} ion effective polarizability, 0.24×10^{-3} nm^3, was obtained by fitting the measured relative intensities in the optical multiplet $^3H_4 \rightarrow {}^3F_3$ at $T > T_N$. The corresponding parameters of the dipole moment (10) equal $b_3^4 = -27.3$, $b_3^6 = 4.24$, and $b_{-6}^6 = -3.98$ (in units of 10^{-5} e nm). The calculated intensities of the transitions from the two lowest sublevels of the ground multiplet $^3H_4$ to the singlet sublevels of the $^3F_3$ multiplet are compared with the experimental data in Table II. One readily sees that $\Gamma_1 \rightarrow \Gamma_1$ and $\Gamma_2 \rightarrow \Gamma_2$ transitions, forbidden in the paramagnetic phase, become allowed in the magnetically ordered phase due to mixing of Γ_1 and Γ_2 states by the exchange interaction. In particular, the intensity of the strong allowed transition $\Gamma_1^{\text{II}}(48\ \text{cm}^{-1}) \rightarrow \Gamma_2^D(6555\ \text{cm}^{-1})$ is partly redistributed at low temperatures between the formerly forbidden transitions $\Gamma_2^{\text{I}}(0) \rightarrow \Gamma_2^D(6555\ \text{cm}^{-1})$ and

TABLE II. Measured and calculated (in brackets) integral intensities (relative units) of electric dipole transitions (π polarization) from the ground and the first excited states to the singlet sublevels of the $^3F_3$ multiplet, devided by the relative population of the initial level. The value of 100 is ascribed to the $\Gamma_1^{II} \rightarrow \Gamma_2^D$ transition.

$^3F_3$ / $^3H_4$	Γ_2^B 6482.5 cm^{-1}		Γ_2^D 6555 cm^{-1}		Γ_1^E 6571.7 cm^{-1}	
	$T>T_N$	$T=5$ K	$T>T_N$	$T=5$ K	$T>T_N$	$T=5$ K
Γ_2^I 0 cm^{-1}	0	1.3 ± 0.4	0	7.2 ± 1.5	6.6 ± 1.3	4.0 ± 1.0
	(0)	(1.3)	(0)	(5.8)	(2.7)	(1.6)
Γ_1^{II} 48 cm^{-1}	20 ± 4	20 ± 4	100	100 ± 20	0	
	(25)	(23.7)	(100)	(91.8)	(0)	(3.5)

$\Gamma_1^{II}(48\ \text{cm}^{-1}) \rightarrow \Gamma_1^E(6571.7\ \text{cm}^{-1})$. Taking into account the measured temperature dependence of the gap between the lowest Γ_1^{II} and Γ_2^I sublevels of the ground multiplet $^3H_4$ and their populations, we can match satisfactorily the observed relative intensities of the allowed $\Gamma_1^{II}(48\ \text{cm}^{-1}) \rightarrow \Gamma_2^B(6482.5\ \text{cm}^{-1})$ and the forbidden $\Gamma_2^I(0) \rightarrow \Gamma_2^B(6482.5\ \text{cm}^{-1})$ transitions at temperatures below T_N.

Note that eigenvalues of Hamiltonian (9) do not depend on the sign of the iron magnetic moment $M_{\text{Fe},z}$ and values of splittings and shifts of spectral lines below T_N are invariant against the transformation $\boldsymbol{F} \rightarrow -\boldsymbol{F}$. The sign of the exchange potential was determined from the analysis of the magnetic susceptibility which is presented in the next section.

V. STATIC MAGNETIC SUSCEPTIBILITY

Let us consider linear responses of the coupled Pr- and Fe-subsystems to the weak external magnetic fields. We have a possibility to compare calculated magnetic moments induced by the external field at different temperatures with the temperature dependences of the principal values of the susceptibility tensor of $PrFe_3(BO_3)_4$ measured in Ref. 12 and hence to check the set of parameters of Hamiltonian (9).

A. Paramagnetic phase

Magnetic properties of the iron subsystem have been considered earlier in Ref. 28 in the framework of the two-particle cluster model. In the mean-field approximation, neglecting the anisotropy energy and the magnetic dipole-dipole interactions (which are about two orders of magnitude smaller than the exchange interaction), we write the Hamiltonian of the two nearest-neighbor Fe^{3+} ions inside the spiral chain with the spin moments $\boldsymbol{S}_1$ and $\boldsymbol{S}_2$,

$$H_d = -2J_{nn}\boldsymbol{S}_1 \cdot \boldsymbol{S}_2 - [2(J_{nn}+2J_{nnn})\langle \boldsymbol{S}_{\text{Fe}}\rangle - g\mu_B(\boldsymbol{B}+\langle \boldsymbol{F}\rangle/3)] \cdot (\boldsymbol{S}_1+\boldsymbol{S}_2). \tag{11}$$

Here, the first term corresponds to the isotropic exchange interaction within this Fe-Fe dimer, the second term represents the exchange interactions of the dimer with the nearest- and next-nearest-neighbor Fe^{3+} ions that belong to the same chain and to the two other neighboring chains, respectively, the third and the fourth terms describe the interaction with the external magnetic field $\boldsymbol{B}$ and the exchange interaction with the nearest Pr^{3+} ions, respectively, (each Fe^{3+} ion has two nearest-neighbor Pr^{3+} ions); J_{nn} and J_{nnn} are the corresponding intrachain and interchain exchange integrals considered as adjustable parameters and $\langle \boldsymbol{F}\rangle$ is defined below. To avoid introduction of additional fitting parameters, we used in this work the values $J_{nn}=-6.25$ K, $J_{nnn}=-1.92$ K obtained in our previous study on the magnetic susceptibility of $NdFe_3(BO_3)_4$.[28]

At temperatures $T>T_N$, average values of the iron spin moments ($\langle \boldsymbol{S}_1\rangle=\langle \boldsymbol{S}_2\rangle=\langle \boldsymbol{S}_{\text{Fe}}\rangle$) and of the operator $\boldsymbol{F}$ are linear in the external field $\boldsymbol{B}$. The magnetic moments of the Fe^{3+} and Pr^{3+} ions induced by the magnetic field equal

$$\boldsymbol{M}_{\text{Fe}} = \chi_d^{\text{Fe}}(\boldsymbol{B}+\langle \boldsymbol{F}\rangle/3),$$

$$\boldsymbol{M}_{\text{Pr}} = -\mu_B\left\langle \sum_k (\boldsymbol{l}_k + 2\boldsymbol{s}_k)\right\rangle = \boldsymbol{\chi}_{\text{Pr}}\boldsymbol{B} + \boldsymbol{\beta}\boldsymbol{M}_{\text{Fe}}, \tag{12}$$

where $\langle \boldsymbol{F}\rangle = \boldsymbol{\beta}\boldsymbol{B} - \boldsymbol{\gamma}\boldsymbol{M}_{\text{Fe}}$ and the symbol $\langle\cdots\rangle$ denotes a thermal average with the Hamiltonian

$$H_{\text{Pr}} = H_{\text{Pr}}^{(p)} + g\mu_B\boldsymbol{F}\cdot\langle \boldsymbol{S}_{\text{Fe}}\rangle + \sum_k \mu_B(\boldsymbol{l}_k+2\boldsymbol{s}_k)\cdot\boldsymbol{B} \tag{13}$$

of the Pr^{3+} ion in the external magnetic field. The analytical expression for the isotropic dimer susceptibility χ_d^{Fe} (per ion) was presented in our previous work [see Eqs. (8)–(10) in Ref. 28]. The components of the axial tensors $\boldsymbol{\beta}$ and $\boldsymbol{\gamma}$ and of the susceptibility tensor $\boldsymbol{\chi}_{\text{Pr}}$ of the Pr^{3+} ion were computed for the temperatures from $T_N=32$ K up to 300 K with a step of one K. The components of the bulk susceptibility (per mole) can be easily obtained from the self-consistent equations (12),

$$\chi_{\lambda\lambda} = N_A\left[\chi_{\text{Pr},\lambda\lambda} + \frac{\chi_d^{\text{Fe}}(3+\beta_{\lambda\lambda})^2}{3+\chi_d^{\text{Fe}}\gamma_{\lambda\lambda}}\right], \tag{14}$$

where N_A is the Avogadro number. The calculated temperature dependences of $\chi_{zz}=\chi_\parallel$ and $\chi_{xx}=\chi_\perp$ are compared with the experimental data[12] in Fig. 11. At temperatures above 200 K the influence of the Pr-Fe exchange interaction is practically negligible and $\chi_{\lambda\lambda} \approx N_A(\chi_{\text{Pr},\lambda\lambda}+3\chi_d^{\text{Fe}})$. However, at lower temperatures the renormalization of the iron dimer

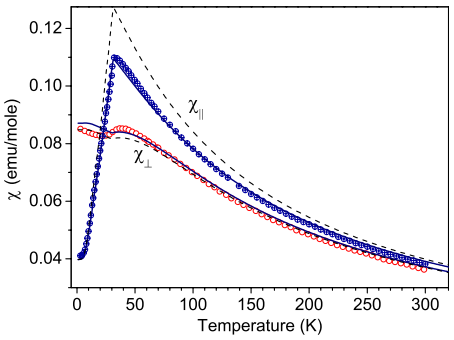

FIG. 11. (Color online) Temperature dependences of the longitudinal and transversal magnetic susceptibilities of $PrFe_3(BO_3)_4$. Symbols—experimental data digitized from Ref. 12; the results of calculations are represented by solid and dashed (for the inverse sign of the Pr-Fe exchange interaction) curves.

susceptibility due to the Pr-Fe interaction results in changes in the calculated $\chi_\parallel$ and $\chi_\perp$ (up to $\pm 7.4\%$ and $\pm 1.2\%$, respectively) depending on the sign of the operator $\boldsymbol{F}$. The set of parameters $a_p^{(q)}$ in Eq. (8) presented in the preceding section provides the best agreement of the calculated susceptibilities with the experimental data (see Fig. 11).

B. Antiferromagnetic phase

The mean-field approximation yields a greatly overestimated phase transition temperature, especially for quasi-one-dimensional systems. As it is well known, a long-range order should be absent in Heisenberg spin chains with finite-range interactions, but we obtain the nonzero $T_N=55$ K for the isolated iron chain in the framework of the dimer model using the intrachain exchange integral J_{nn} given above.[28] To solve this problem, we modify the model deleting the terms in the effective dimer Hamiltonian which are responsible for the formation of the long-range order in the single iron chain. At temperatures $T<T_N$ and in absence of the external magnetic field, the Hamiltonian of an iron dimer is written in the following form

$$H_d(M) = -2J_{nn}\boldsymbol{S}_1\cdot\boldsymbol{S}_2 + g\mu_B\left(\frac{1}{3}\langle F_z\rangle + \frac{4J_{nnn}}{(g\mu_B)^2}M\right)(S_{1,z}-S_{2,z}), \tag{15}$$

where $M=g\mu_B\langle S_{1z}\rangle_0=-g\mu_B\langle S_{2z}\rangle_0$ (the symbol $\langle\cdots\rangle_0$ denotes a thermal average with the Hamiltonian $H_d(M)$) and $\langle F_z\rangle$ is the operator F_z averaged with the Hamiltonian $H_{\mathrm{Pr}}^{(+)}$ [see Eq. (9)]. Using Hamiltonian (15), we obtain the isotropic staggered susceptibility of the iron subsystem (for $\langle F_z\rangle=0$),

$$\chi_{\mathrm{Fe}}^{AF}(T) = \frac{N_A(g\mu_B)^2}{2\{2J_{nnn}-3J_{nn}Z(T)[36-Z(T)]^{-1}\}}, \tag{16}$$

($Z(T)=\Sigma_{S=0}^{5}(2S+1)\exp[S(S+1)J_{nn}/k_BT]$ is the statistical sum for the isolated dimer) which diverges at $T_N=36$ K. So, in the framework of the modified dimer model used in the present work, the phase transition is induced by the interchain exchange interactions only, and the transition temperature agrees well with the experimental data for different RE iron borates.

The dimer susceptibility is anisotropic in the ordered phase. The Hamiltonian of an iron dimer in the external magnetic field $\boldsymbol{B}$ reads

$$H_d(M,\boldsymbol{B}_{\mathrm{eff}}) = H_d(M) + g\mu_B\boldsymbol{B}_{\mathrm{eff}}\cdot(\boldsymbol{S}_1+\boldsymbol{S}_2), \tag{17}$$

where the effective magnetic field equals $\boldsymbol{B}_{\mathrm{eff}}=\boldsymbol{B}+J_t\delta\boldsymbol{M}_{\mathrm{Fe}}+\delta\langle\boldsymbol{F}\rangle/3$ with $J_t=2(J_{nn}+2J_{nnn})/(g\mu_B)^2$ and

$$\delta\langle F_\lambda\rangle = \frac{\mathrm{Tr}[(F_\lambda-\langle F_z\rangle\delta_{\lambda z})\exp(-H_{\mathrm{Pr}}^{(+)}(\boldsymbol{B},\delta\boldsymbol{M}_{\mathrm{Fe}})/k_BT)]}{\mathrm{Tr}\exp(-H_{\mathrm{Pr}}^{(+)}(\boldsymbol{B},\delta\boldsymbol{M}_{\mathrm{Fe}})/k_BT)}. \tag{18}$$

Here $H_{\mathrm{Pr}}^{(+)}(\boldsymbol{B},\delta\boldsymbol{M}_{\mathrm{Fe}})$ is the Hamiltonian of the Pr^{3+} ions at $T<T_N$ in the external magnetic field,

$$H_{\mathrm{Pr}}^{(+)}(\boldsymbol{B},\delta\boldsymbol{M}_{\mathrm{Fe}}) = H_{\mathrm{Pr}}^{(+)} - \boldsymbol{F}\cdot\delta\boldsymbol{M}_{\mathrm{Fe}} + \sum_k \mu_B(\boldsymbol{l}_k+2\boldsymbol{s}_k)\cdot\boldsymbol{B}. \tag{19}$$

Thus, we have neglected the intrachain interactions between iron dimers in Hamiltonian (15) for zero external magnetic field, but, in Hamiltonian (17), we save all terms corresponding to interactions of a dimer with the magnetic moments of the nearest and next-nearest iron ions induced by the external field.

In the linear approximation, we obtain for $\delta\langle\boldsymbol{F}\rangle$ and for magnetic moments of the Fe^{3+} ($\delta\boldsymbol{M}_{\mathrm{Fe}}$) and Pr^{3+} ($\delta\boldsymbol{M}_{\mathrm{Pr}}$) ions induced by the external magnetic field a system of self-consistent equations similar to Eq. (12). Expression (14) for the bulk susceptibility at $T>T_N$ is valid at $T<T_N$ as well, however, in the latter case the components of the axial tensors $\boldsymbol{\beta}$, $\boldsymbol{\gamma}$ and $\boldsymbol{\chi}_{\mathrm{Pr}}$ are computed by making use of Hamiltonian (19), and the susceptibility of the iron ions χ_d^{Fe} is replaced by $\chi_{d,\lambda\lambda}^{\mathrm{Fe}}=\chi_{\lambda\lambda}^{\mathrm{Fe}}(1-\chi_{\lambda\lambda}^{\mathrm{Fe}}J_t)^{-1}$, where

$$\chi_{\lambda\lambda}^{\mathrm{Fe}} = -\lim_{\boldsymbol{B}\to 0}\frac{g\mu_B}{2B_\lambda}\mathrm{Tr}[(S_{1,\lambda}+S_{2,\lambda}) \times\exp(-H_d(M,\boldsymbol{B})/k_BT)]/\mathrm{Tr}\exp(-H_d(M,\boldsymbol{B})/k_BT). \tag{20}$$

The results of calculations carried out for fixed temperatures T (with the step of one K) using the measured values of the order parameter $M(T)$ agree well with the temperature dependences of the longitudinal and transversal susceptibilities presented in Ref. 12 (see Fig. 11).

VI. SUMMARY

High-resolution (0.1 cm^{-1}) broadband (1500–23 000 cm^{-1}) temperature-dependent polarized optical absorption spectra of the $PrFe_3(BO_3)_4$ single crystals, pure and with 1% of erbium introduced as a spectroscopic probe, have been measured. The energies and symmetries of the 54 CF levels have been found from the analysis of the spectra of $PrFe_3(BO_3)_4$ in the paramagnetic phase and compared with the results of crystal-field calculations that took into account the $4f^2/4f5d$ and $4f^2/4f6p$ configuration interactions. This procedure resulted in a set of six CF parameters for the ground $4f^2$ configuration of Pr^{3+} in the D_3 symmetry site of $PrFe_3(BO_3)_4$.

The spectra of Er^{3+} probe in $PrFe_3(BO_3)_4$ point unambiguously to the magnetic phase transition at $T_N=32$ K into the antiferromagnetic structure of the easy-axis type. The splitting of the Γ_3 doublets and level shifts due to the Pr-Fe exchange interaction in the magnetically ordered phase have been measured and analyzed using the exchange Hamiltonian parametrized by seven parameters. An important result of this analysis is that the anisotropic terms in the exchange Hamiltonian are comparable with or even greater than the isotropic term. The calculated magnetic moments of the Pr^{3+} ions induced by the exchange interaction with the magnetically ordered iron subsystem at low temperatures saturate at the value of 0.95 μ_B and are antiparallel to magnetic moments of the nearest-neighbor Fe^{3+} ions.

An interesting effect has recently been observed[30] in the low-temperature spectra of $PrFe_3(BO_3)_4$, namely, strictly forbidden spectral lines emerge at the magnetic ordering temperature and grow in intensity when further lowering the temperature. We show that this effect takes place due to the mixing of Pr^{3+} singlet states by the exchange interaction in the magnetically ordered phase and describe it quantitatively using our model of crystal-field and exchange interactions. The developed model was tested also by comparing the calculated temperature dependences of the longitudinal and transversal magnetic susceptibilities with the experimental data.

In summary, the obtained in this work set of six CF parameters and seven parameters of the exchange interaction between the praseodymium and iron subsystems allows us to describe satisfactorily the spectral and magnetic properties of $PrFe_3(BO_3)_4$ in the paramagnetic and antiferromagnetic phases. The results of the present study also confirm that the model of the iron dimers inside the spiral chains of $Fe^{3+}(O^{2-})_6$ octahedrons introduced earlier in Ref. 28 and modified in the present work may serve as a basis for the analysis of low-temperature properties of other RE iron borates.

ACKNOWLEDGMENTS

We thank S. Klimin for useful information concerning the structure of $PrFe_3(BO_3)_4$ and E. Chukalina for participating in some measurements. This work was supported in part by the Russian Foundation for Basic Research (Grants No. 07-02-01185 and No. 09-02-00930) and by the Russian Academy of Sciences under the Programs for Basic Research.

[1] N. I. Leonyuk and L. I. Leonyuk, Prog. Cryst. Growth Charact. Mater. **31**, 179 (1995).
[2] B. Lu, J. Wang, H. Pan, M. Jiang, E. Liu, and X. Hou, J. Appl. Phys. **66**, 6052 (1989).
[3] D. Jaque, J. Capmany, and J. G. Sole, Appl. Phys. Lett. **75**, 325 (1999).
[4] P. Dekker and J. M. Dawes, Opt. Express **12**, 5922 (2004).
[5] L. N. Bezmaternykh, S. A. Kharlamova, and V. L. Temerov, Crystallogr. Rep. **49**, 855 (2004).
[6] A. D. Balaev, L. N. Bezmaternykh, I. A. Gudim, V. L. Temerov, S. G. Ovchinnikov, and S. A. Kharlamova, J. Magn. Magn. Mater. **258-259**, 532 (2003).
[7] N. Tristan, R. Klinger, C. Hess, B. Buchner, E. Popova, I. A. Gudim, and L. N. Bezmaternykh, J. Magn. Magn. Mater. **316**, e621 (2007).
[8] E. A. Popova, D. V. Volkov, A. N. Vasiliev, A. A. Demidov, N. P. Kolmakova, I. A. Gudim, and L. N. Bezmaternykh, Phys. Rev. B **75**, 224413 (2007).
[9] E. A. Popova, N. Tristan, A. N. Vasiliev, V. L. Temerov, L. N. Bezmaternykh, N. Leps, B. Buchner, and R. Klinger, Eur. Phys. J. B **62**, 123 (2008).
[10] A. K. Zvezdin, S. S. Krotov, A. M. Kadomtseva, G. P. Vorob'ev, Y. F. Popov, A. P. Pyatakov, L. N. Bezmaternykh, and E. A. Popova, JETP Lett. **81**, 272 (2005).
[11] A. K. Zvezdin, G. P. Vorob'ev, A. M. Kadomtseva, Yu. F. Popov, A. P. Pyatakov, L. N. Bezmaternykh, A. V. Kuvardin, and E. A. Popova, JETP Lett. **83**, 509 (2006).
[12] A. M. Kadomtseva, Yu. F. Popov, G. P. Vorob'ev, A. A. Mukhin, V. Yu. Ivanov, A. M. Kuz'menko, and L. N. Bezmaternykh, JETP Lett. **87**, 39 (2008).
[13] F. Yen, B. Lorenz, Y. Y. Sun, C. W. Chu, L. N. Bezmaternykh, and A. N. Vasiliev, Phys. Rev. B **73**, 054435 (2006).
[14] P. Fischer, V. Pomjakushin, D. Sheptyakov, L. Keller, M. Janoschek, B. Roessli, J. Schefer, G. Petrakovskii, L. Bezmaternikh, V. Temerov, and D. Velikanov, J. Phys.: Condens. Matter **18**, 7975 (2006).
[15] D. Fausti, A. Nugroho, P. van Loosdrecht, S. A. Klimin, M. N. Popova, and L. N. Bezmaternykh, Phys. Rev. B **74**, 024403 (2006).
[16] S. A. Klimin (upublished).
[17] S. A. Klimin, D. Fausti, A. Meetsma, L. N. Bezmaternykh, P. H. M. van Loosdrecht, and T. T. M. Palstra, Acta Crystallogr., Sect. B: Struct. Sci. **61**, 481 (2005).
[18] Y. Hinatsu, Y. Doi, K. Ito, M. Wakeshima, and A. Alemi, J. Solid State Chem. **172**, 438 (2003).
[19] E. P. Chukalina, D. Yu. Kuritsin, M. N. Popova, L. N. Bezmaternykh, S. A. Kharlamova, and V. L. Temerov, Phys. Lett. A **322**, 239 (2004).
[20] A. M. Kadomtseva, V. Yu. Ivanov, A. A. Mukhin, Yu. F. Popov, G. P. Vorob'ev, A. M. Kuzmenko, A. P. Pyatakov, A. K. Zvezdin, A. S. Prokhorov, and L. N. Bezmaternikh, Book of Abstracts: Moscow International Symposium on Magnetism, Moscow, 20–25 June 2008, pp. 625–626.
[21] R. Z. Levitin, E. A. Popova, R. M. Chtsherbov, A. N. Vasiliev, M. N. Popova, E. P. Chukalina, S. A. Klimin, P. H. M. van Loosdrecht, D. Fausti, and L. N. Bezmaternykh, JETP Lett. **79**, 423 (2004).
[22] A. I. Pancratz, G. A. Petrakovskii, L. N. Bezmaternykh, and O. A. Bayukov, JETP **99**, 766 (2004).
[23] H. Mo, Ch. Nelson, L. N. Bezmaternykh, and V. T. Temerov, Phys. Rev. B **78**, 214407 (2008).
[24] T. N. Stanislavchuk, E. P. Chukalina, M. N. Popova, L. N. Bezmaternykh, and I. A. Gudim, Phys. Lett. A **368**, 408 (2007).
[25] C. Ritter, A. Vorotynov, A. Pankrats, G. Petrakovskii, V. Te-

merov, I. Gudim, and R. Szymczak, J. Phys.: Condens. Matter **20**, 365209 (2008).
[26] M. N. Popova, E. P. Chukalina, T. N. Stanislavchuk, and L. N. Bezmaternykh, J. Magn. Magn. Mater. **300**, e440 (2006).
[27] C. Ritter, A. Balaev, A. Vorotynov, G. Petrakovskii, D. Velikanov, V. Temerov, and I. Gudim, J. Phys.: Condens. Matter **19**, 196227 (2007).
[28] M. N. Popova, E. P. Chukalina, T. N. Stanislavchuk, B. Z. Malkin, A. R. Zakirov, E. Antic-Fidancev, E. A. Popova, L. N. Bezmaternykh, and V. L. Temerov, Phys. Rev. B **75**, 224435 (2007).
[29] P. M. Levy, Phys. Rev. **135**, A155 (1964).
[30] M. N. Popova, T. N. Stanislavchuk, B. Z. Malkin, and L. N. Bezmaternykh, Phys. Rev. Lett. **102**, 187403 (2009).
[31] A. de Andres, F. Agullo-Rueda, S. Taboada, C. Cascales, J. Campa, C. Ruiz-Valero, and I. Rasines, J. Alloys Compd. **250**, 394 (1997).
[32] B. Z. Malkin, *Spectroscopic Properties of Rare Earths in Optical Materials*, Springer Series in Materials Science Vol. 83, edited by G. Liu and B. Jacquier, (Springer, Berlin, 2005), pp. 130–190.
[33] M. N. Popova, J. Alloys Compd. **275-277**, 142 (1998).
[34] O. K. Moune, M. D. Faucher, and N. Edelstein, J. Alloys Compd. **323-324**, 783 (2001).
[35] M. D. Faucher and O. K. Moune, Phys. Rev. A **55**, 4150 (1997).
[36] C. K. Jorgensen and B. R. Judd, Mol. Phys. **8**, 281 (1964).